1. Current Drive in the Presence of Bootstrap Current in Tokamaks

Sponsors:

Department of Energy
Grant DE-FG02-91ER-54109

Project Staff:

Steven D. Schultz, Prof. Abraham Bers, Dr. Abhay K. Ram

Steady-state operation of tokamak fusion energy reactors requires non-inductive current generation in the plasma for its confinement. It has been proposed that RF current drive in combination with the bootstrap current may achieve this goal.[1] Here we report on the main results of a study on the interaction of RF current drive (lower hybrid, LHCD, and electron cyclotron, ECCD) with the bootstrap current in a tokamak plasma. By calculating RF current drive and bootstrap current in a self-consistent kinetic manner, we find synergistic effects in the total noninductive current. Although the synergistic effects are relatively small, they are positive and may be significant in profile control of the total current for overall plasma stability.

The formulation of the problem entailed including quasilinear diffusion (due to RF waves in the plasma) in the neoclassical drift-kinetic equation for plasma transport, and generating an appropriate relativistic code in two-dimensional momentum space (FASTFP-NC)[2] for evaluating both RF-driven current and bootstrap current independently, and together self-consistently. To make the analysis and computations manageable, the formulation and code were limited to the thin banana regime for electrons, and the study restricted to finding the currents on a single flux surface with given plasma parameters, including specified density and temperature gradients.

(a) LHCD and Bootstrap Current

For this scenario, we describe the results using Alcator C-MOD type parameters (under a possible "advanced tokamak" operation). Calculations were performed at $r = 0.15$ m $(\epsilon = 0.23)$, and with a normalized quasilinear diffusion coefficient $D_0 = 4$ for a flat spectrum of waves in the range of parallel phase velocities $3.5v_{Te} \leq v_{\|} \leq 6.0v_{Te}$. In the absence of the LH fields, and with the local distribution function an unperturbed maxwellian, we obtained a flux surface averaged bootstrap current $\langle J_{\|}^{B} B\rangle/\langle B\rangle = 2.9MA/\mathrm{m}^2$, where the superscript B on $J_{\|}$ denotes that this is the bootstrap current in the absence of RF. Ignoring the bootstrap current, we found that LHCD alone was $J_{\|}^{L} = 10.6MA/\mathrm{m}^2$. The total self-consistent noninductive current (LHCD in the presence of bootstrap current) was $\langle J_{\|} B\rangle/\langle B\rangle = 14.0MA/\mathrm{m}^2$. Defining the synergistic current density as

$$J_{\|}^{S} = J_{\|} - (J_{\|}^{B} + J_{\|}^{L}) \,, \tag{1}$$

this case gave $J_{\|}^{S} \approx 500kA/\mathrm{m}^2$ of synergistic current density. The synergistic current can be understood by looking at the modifications of the usual parallel LHCD distribution function due to the presence of bootstrap current, and at the modifications of the perturbed parallel distribution function of bootstrap current in the presence of LHCD. The former, shown in Figure 1, compares

[1] A. Bers and A. K. Ram, "Lower Hybrid and Fast Wave Current Drive—Status of Theory," in *Proceedings of the IAEA Technical Meeting on Fast Wave Current in Reactor Scale Tokamaks (Synergy and Complementarity with LHCD and ECRH)*, Arles, France, 23–25 September 1991, eds. D. Moreau, A. Bécoulet, and Y. Peysson, pp. 2–34; and M. Kikuchi, "Prospects of a Stationary Tokamak Reactor," *Plasma Phys. Contr. Fusion,* **35**, B39 (1993).

[2] Steven D. Schultz, "Lower Hybrid and Electron Cyclotron Current Drive With Bootstrap Current in Tokamaks," Ph.D. thesis, Department of Physics, M.I.T., September, 1999.

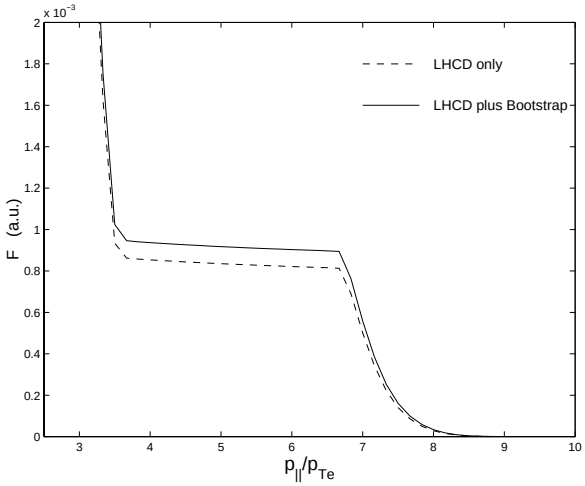

Figure 1: Parallel distribution function $F = \int 2\pi p_\perp dp_\perp f$ for LHCD as a function of $p_\parallel / p_{Te}$, with RF only (dashed line) and with RF plus bootstrap current (solid line). Parameters are Alcator C-Mod type with $r = 0.15$ m, $D_0 = 4.0$ for $v_\parallel \in (3.5 v_{Te}, 6.0 v_{Te})$.

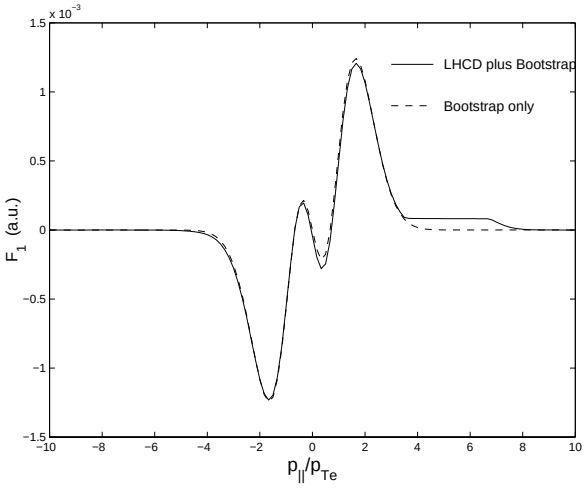

Figure 2: Perturbed parallel distribution function $F_1 = \int 2\pi p_\perp dp_\perp (\tilde{f} + g)$ for LHCD as a function of $p_\parallel / p_{Te}$, with bootstrap current only (dashed line) and bootstrap with LH (solid line). Parameters are Alcator C-Mod type with $r = 0.15$ m, $D_0 = 4.0$ for $v_\parallel \in (3.5 v_{Te}, 6.0 v_{Te})$.

the self-consistent LHCD plus bootstrap distribution $F = \int dp_\perp 2\pi p_\perp [f_0 + \tilde{f} + g]$ to $F_0 = \int dp_\perp 2\pi p_\perp f_0$ which is the distribution function for LHCD in the absence of bootstrap current. The latter is shown in Figure 2 and compares F with the parallel, perturbed distribution function $F_1 = \int dp_{\perp 0} 2\pi p_{\perp 0} [\tilde{f} + g]$ which gives the bootstrap current in the absence of LHCD.

The synergistic increase in current density due to the bootstrap current enhancement of the LHCD plateau can be estimated analytically. In the far circulating region of phase space, where the LH spectrum of waves interact with electrons, the added height of the plateau can be estimated from F_1 evaluated at the lower limit of the LH spectrum, $(v_\parallel)_{\min} \equiv v_1$. We thus find approximately,

$$\frac{J_\parallel^S}{J_\parallel^L} \approx \frac{\sqrt{\epsilon}}{2} \rho_\theta \frac{d \ln T_e}{dr} \left(\frac{v_1}{v_{Te}} \right)^3 , \tag{2}$$

where $\epsilon = (r/R)$, $\rho_\theta = v_{Te}/\Omega_\theta$ is the poloidal gyroradius, and T_e is the electron temperature. To test this, we have carried out a series of computations using FASTFP-NC on a variety of parameters for both Alcator C-MOD type tokamak plasmas and ARIES-RS tokamak type plasmas. We find that although (2) can predict the FASTFP-NC computations only within a factor of two, it gives the correct scaling of the synergistic LH-bootstrap current with plasma parameters. From (2) we surmise that the synergistic current density increases with the parallel phase velocity (relative to electron thermal velocity) of the lower end of the LH wave spectrum, and with bootstrap current density relative to $en_e v_{Te}$. LH wave absorption by Landau damping places $(v_1/v_{Te}) \approx 3 - 4$; the increase of the synergism with bootstrap current is borne out by computations showing that essentially a doubling of the bootstrap current density resulted in a doubling of the synergistic current density.

(b) ECCD and Bootstrap Current

The interaction of electron cyclotron current drive with bootstrap current is more complicated. Since EC waves are absorbed at parallel phase velocities close to the electron thermal velocity, their interaction with trapped electrons leads in general to an ECCD figure of merit lower than for LHCD. For this reason, one would also expect a more significant interaction of ECCD with bootstrap current; however, at low parallel phase velocities, the Ohkawa effect[3] becomes detrimental to ECCD. To study these effects, we carried out a series of computations with FASTFP-NC for DIII-D tokamak type parameters. Calculations were performed for second-harmonic X-mode ECCD with an effective, normalized, bounce-averaged, quasilinear diffusion coefficient[4] $D_0 = 0.4$, for various parallel indices $N_\parallel = (ck_\parallel/\omega)$. The results show that the total current density increases with $N_\parallel$, owing to the greater penetration of the waves into the bulk of the electron distribution function, until the Ohkawa effect starts to reduce the current density; the synergistic current density, however, increases with $N_\parallel$ even when the Ohkawa effect appears. In contrast to the mildly appreciable synergism observed with LHCD, at relatively low bootstrap current densities in DIII-D the ECCD synergism is only 2% or less than the total current density. To see the effects of appreciable bootstrap current density, a hypothetical ECCD scenario for advanced operation Alcator C-MOD tokamak type parameters ($B_\zeta = 4T$, $T_e = 7.5$ keV, $J_\parallel^B = 2.9 MA/\mathrm{m}^2$) with the same $D_0 = 0.4$ shows that the synergistic current density is much more substantial ($J_\parallel^S/J_\parallel^C \approx 22\%$). Computations using the ARIES-RS tokamak type parameters showed the synergistic currents to be considerably lower than for the best Alcator C-MOD cases.

The detailed structure of the synergism for ECCD bootstrap current is more difficult to analyze. The most striking difference in the electron distribution function compared to its nearly maxwellian

[3] T. Ohkawa, "Steady State Operation of Tokamaks by RF Heating," *General Atomics Company Report No. A13847* (1976).

[4] R. A. Cairns and C. Lashmore-Davies, "Flux Surface Averaging of the Diffusion Coefficient in Electron Cyclotron Resonance Heating," *Plasma Phys. and Cont. Fusion,* **28**, 1539 (1986); M. Shoucri and I. Shkarofsky, "A Fokker-Planck Code for the Electron-Cyclotron Current Drive and Electron-Cyclotron/Lower Hybrid Current Drive Synergy," *CCFM Report 467* (1996).

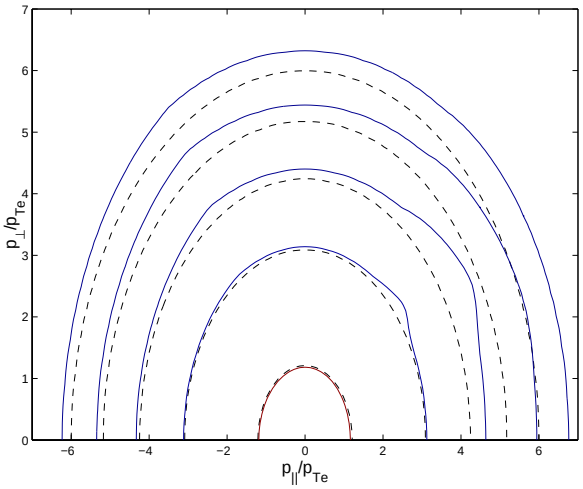

Figure 3: Contour plot in $(p_{\|}/p_{Te}, p_{\perp}/p_{Te})$ space of the EC-modified electron distribution function (solid contours) and the Maxwellian distribution unmodified by EC (dashed contours). Parameters are DIII-D type with $r = 0.3$ m, $2\Omega_0/\omega = 0.96$, $N_{\|} = 0.35$, and $D_0 = 0.4$.

form in the absence of EC waves, shown in Figure 3, is the effect of an increased electron temperature due to EC waves. The increase in electron temperature (ΔT_e) and its radial gradient give a direct increase in the bootstrap current. Taking the resultant (non-maxwellian) electron distribution function, f, from FASTFP-NC and calculating an effective electron temperature from $T_e = \int d^3p(1/2)(p^2/\gamma m_e)f/(3/2n_e)$, we can determine (ΔT_e), and using the general bootstrap current formula,[5] we can then find the change in bootstrap current due to (ΔT_e) as

$$\langle(\Delta J_{\|}^{B})B\rangle = -p_e\frac{B_\zeta}{B_\theta}\left[L_{31}\frac{d(\ln n_e)}{dr} + (L_{31}+L_{32})\frac{d(\ln \Delta T_e)}{dr}\right]\frac{\Delta T_e}{T_e} \tag{3}$$

where we assume that the transport coefficients L_{31} and L_{32} are unchanged due to EC waves. The predictions from (3) are found to be in reasonable agreement with $J_{\|}^{S}$ calculated from FASTFP-NC.

Further details of this study can be found in the Ph.D. thesis of Steven D. Schultz.[2]

[5] F. L. Hinton and R. D. Hazeltine, "Theory of Plasma Transport in Toroidal Confinement Systems," *Rev. Mod. Phys.,* **48**, 239 (1976); S. P. Hirshman and D. J. Sigmar, "Neoclassical Transport of Impurities in Tokamak Plasmas," *Nucl. Fusion,* **21**, 1079 (1981).

2. Electron Bernstein Waves in NSTX and MAST-Type Plasmas

Sponsors:

Department of Energy/National Spherical Tokamak Experiment
Grant DE-FG02-99ER-54521

Project Staff:

Dr. Abhay K. Ram, Prof. Abraham Bers, Dr. C. N. Lashmore-Davies

In high-β, low magnetic field spherical tokamaks, electron Bernstein waves in the electron cyclotron range of frequencies can be useful for heating and driving non-inductive plasma currents as well as a diagnostic for determining electron temperatures. The nature of spherical tokamak plasmas (e.g., NSTX in the U.S. and MAST in the U.K.) does not allow for the conventional electron cyclotron waves — the ordinary O-mode and the extraordinary X-mode — to be effective means for heating, driving currents, or diagnosing electron temperatures. These limitations can be overcome by coupling external power in the electron cyclotron range of frequencies to electron Bernstein waves (EBW). Our initial studies on such coupling were previously reported.[6] During the past year, these studies were refined and more specifically applied to realizations in NSTX and MAST, in collaborative work with these experiments. Here we summarize the main results.

The coupling to EBWs can be indirect or direct. The indirect coupling is through mode conversion of slow X-mode to the EBW at the upper hybrid resonance (UHR). The coupling to the slow X-mode is through the vacuum modes: the fast X-mode or the O-mode which can be directly excited from outside the plasma. The former is referred to as the X-B mode conversion and the latter as the O-X-B mode conversion process. We have developed analytical and numerical techniques for studying both conversion processes.[7,8]

From the analytical analysis, we find that the mode conversion efficiency is dependent on

$$\eta \approx \frac{\omega_{ce} L_n}{c\alpha} \left[\sqrt{1+\alpha^2} - 1\right]^{1/2} \tag{4}$$

where all quantities on the right-hand-side are evaluated at the UHR: L_n is the density scale length, c is the speed of light, and $\alpha = \omega_{pe}/\omega_{ce}$, ω_{pe} and ω_{ce} being the electron plasma and cyclotron frequencies, respectively.

For maximum X-B mode conversion, we find that the X-mode should be propagating essentially across the magnetic field [i.e., $n_\parallel \ll 1$ where $n_\parallel$ is the wave index $(ck_\parallel/\omega)$ parallel to the magnetic

[6] A. Bers, A. K. Ram, V. Fuchs, J. Theilhaber, R. J. Focia, A. Salcedo, S. D. Schultz, and L. Kang, "Plasma Wave Interactions—RF Heating and Current Generation," *Progress Report No. 141,* MIT Research Laboratory of Electronics, Cambridge, 1999, pp. 231–241 .

[7] K. C. Wu, A. K. Ram, A. Bers, and S. D. Schultz, "Electron Cyclotron Heating in NSTX," *Proceedings of the 12th Topical Conference on Radio Frequency Power in Plasmas,* Savannah, Georgia, April 1–3, 1997, A.I.P. Conf. Proc. 403 (eds. P. M. Ryan and T. Intrator), Woodbury, New York (1997), pp. 207–210; A. Bers, A. K. Ram, and S. D. Schultz, "Coupling to Electron Bernstein Waves in Tokamaks," *Proceedings of the 2nd Europhysics Topical Conference on RF Heating and Current Drive of Fusion Devices,* Brussels, Belgium, January 20–23, 1998, eds. J. Jacquinot, G. Van Oost, and R. R. Weynants (Contributed Papers, European Physical Society, Vol. 22A, Petit-Lancy, Switzerland), pp. 237–240; and S. D. Schultz, A. K. Ram, and A. Bers, "Mode-Converted Electron Bernstein Waves for Heating and Current Drive in NSTX," paper IAEA-F1-CN-69/CDP/13, in *Proceedings of the 17th International Atomic Energy Agency Fusion Energy Conference,* Yokohama, Japan, October 19–24, 1998, on CD-ROM at <http://www/iaea/org/programmes/ripc/physics/start.htm>.

[8] A. K. Ram, "Electron Bernstein Wave Excitation in NSTX-Type High-β Plasmas," *Proceedings of the 13th Topical Conference on Radio Frequency Power in Plasmas,* Annapolis, Maryland, April 12–14, 1999, A.I.P. Conf. Proc. 485 (eds. S. Bernabei and F. Paoletti), Woodbury, New York (1999), pp. 375–382.

field]. Then, for a given plasma configuration, the maximum power mode conversion efficiency (at $n_\parallel \approx 0$) is

$$C_{\max} = 4e^{-\pi_\eta}(1 - e^{-\pi_\eta}) \; . \tag{5}$$

For $C_{\max} \gtrsim 0.5$, we require that $0.05 \lesssim \eta \lesssim 0.6$.

The O-X-B mode conversion process is most efficient when the O-mode cutoff coincides with slow X-mode cutoff. This occurs at a critical $n_\parallel$:

$$(n_\parallel)_{\rm crit} = \frac{1}{\sqrt{1+\alpha}} \; . \tag{6}$$

Furthermore, in order to avoid coupling power to the outgoing fast X-mode, we require that $\eta > 1$. From these conditions, we find that the X-B and the O-X-B mode conversion processes optimize in different regions of frequency and $n_\parallel$ space.

We have developed a comprehensive numerical package for solving for mode conversion to EBWs. The numerical scheme treats EBW as a resonance absorption process at the UHR in which the plasma is treated as a cold medium. A more detailed kinetic scheme has also been developed in which the EBW is a wave propagating from mode conversion into the core of the plasma. The results from the two numerical schemes are essentially the same, showing the near-equivalence of studying EBW mode conversion by resonance absorption at the UHR.

We have studied mode conversion in NSTX-type high-β equilibria.[7] For an edge magnetic field of $0.28\,T$ and a density profile of the form $(1 - r^2/a^2)^{1/2}$ where $a = 0.44\,\mathrm{m}$ is the minor radius, the edge density is $6 \times 10^{17}\,\mathrm{m}^{-3}$, and the peak density is $3 \times 10^{19}\,\mathrm{m}^{-3}$, we obtain the following results. The X-B mode conversion frequency is greater than 50% in the frequency range $13 \lesssim f \lesssim 18$ GHz for $n_\parallel = 0$, with an efficiency of 100% for $f = 15$ GHz. For $f = 15$ GHz, the efficiency is greater than 50% for $0 \lesssim n_\parallel \lesssim 0.35$. The O-X-B mode conversion efficiency is 100% for $f = 28$ GHz and $(n_\parallel)_{\rm crit} \approx 0.48$. The range of $n_\parallel$'s for which the efficiency is greater than 50% is $0.4 \lesssim n_\parallel \lesssim 0.6$.

For MAST-type parameters with an edge magnetic field of $0.37\,T$, an edge density of $4 \times 10^{19}\,\mathrm{m}^{-3}$, and a fixed source frequency of 60 GHz, we find that, for $n_\parallel = 0$, the X-B conversion efficiency of 100% is possible if $L_n \approx 1.7 \times 10^{-3}\,\mathrm{m}$ at the UHR. This corresponds to a density profile of the form $(1 - r^2/a^2)^{0.25}$. For optimizing the O-X-B mode conversion, a scale length of $L_n \approx 6 \times 10^{-2}\,\mathrm{m}$ at the UHR for a $(n_\parallel)_{\rm crit} \approx 0.4$ is required.

Direct coupling to EBWs is possible using a slow wave structure which generates, essentially, a radial electric field. This is because the EBWs are, approximately, electrostatic waves. The slow wave structure needs to be placed inside the plasma beyond the slow X-mode cutoff so as not to couple any power to this mode. For NSTX-type parameters and $f = 15$ GHz, the coupling structure needs to be only a few millimeters inside the plasma near the edge. The EBW wave impedance is then approximately one-tenth of the free-space wave impedance.

We have also studied the propagation and damping of EBWs in model spherical tokamak profiles using our general ray tracing code.[9] We find that the EBWs damp very strongly at the Doppler-shifted electron cyclotron resonance or its harmonics. The damping is highly localized and the spatial location of the damping can be controlled by an appropriate placement of the launcher in the poloidal plane. The $n_\parallel$'s along the EBW rays can vary over a large range for rays launched off the equatorial plane. EBWs launched with $n_\parallel \approx 0$ can undergo significant upshifts so that near damping, $|n_\parallel| > 1$. This has important consequences for current drive. While for $|n_\parallel| < 1$ the diffusion paths are hyperbolas and wave-particle resonances are ellipses (as in the case of conventional ECRH), for $|n_\parallel| > 1$ the diffusion paths are ellipses and the wave-particle resonances

[9] A. K. Ram and A. Bers, "Propagation and Damping of Mode Converted Ion-Bernstein Waves in Toroidal Plasmas," *Phys. Fluids B, Plasma Physics,* **3**, 1059 (1991).

are hyperbolas. This can lead to possibly better current drive efficiency than for the conventional ECRF-driven currents.

The localized, strong absorption of EBWs at the Doppler shifted electron cyclotron resonance and its harmonics also makes them a useful means for diagnosing the electron temperature.[10] In order to "observe" this emission in the vacuum edge of the spherical tokamaks, the EBWs have to mode-convert to either the X-mode or the O-mode. While this mode conversion is inherently different from the mode conversion process exciting the EBWs, the kinetic numerical code can be used to determine the conversion efficiency to the X- and O-modes. This can then be related to the black-body temperature of the localized layer where the observed frequency matches the cyclotron resonance (or its harmonics) inside the plasma.

[10] P. C. Efthimion, G. Taylor, B. Jones, J. Spaleta, J. Menard, T. Munsat, J. C. Hosea, R. Kaita, and R. Majeski, "Measurement of Local Electron Temperature in an Overdense Plasma Based Upon Mode-Converted Electron Bernstein Waves (EBW)," *Bull. Am. Phys. Soc.,* **44**, 186 (1999).

3. Enhanced, Localized Fields in Density Gradients and Ion Energization in Space Plasmas

Sponsors:

National Science Foundation
Grant ATM 98-06328
Department of Energy/National Science Foundation
Grant DE-FG02-99ER54555

Project Staff:

Dr. Abhay K. Ram, Prof. Abraham Bers

There are two events that are particularly ubiquitous in space plasmas. One is the existence of short scale-length (of the order of a few ion Larmor radii) density gradients and the other is transverse (to the geomagnetic field) energization of ionospheric ions which, eventually, make their way into the outer reaches of the terrestrial magnetosphere. Observations from TOPAZ, AMICIST, and PHAZE II have shown the existence of density depleted structures in the auroral ionosphere which are associated with enhanced electric fields.[11,12,13,14,15] These structures are a few tens of meters in width transverse to the geomagnetic field and are believed to be of the order of 100 km along the geomagnetic field. Associated with these enhanced fields, transversely accelerated ions with energies in the range of tens of eV are observed.[12,13,14] These energies should be compared to the ambient thermal energies of approximately 0.3 eV. More recently, FAST observations have shown the existence of solitary electric fields in the auroral regions where the dimensions of the field structures, along the geomagnetic fields, are small compared to the ion Larmor radius.[16] The transverse dimensions of these structures have not been completely determined. However, these structures have also been observed to lead to ion energization.

In the past year, we have initiated two studies aimed at understanding these observations. The first seeks to model the occurence of enhanced fields in density gradients; the second attempts to explain the observed ion energization in such fields. We report on both of these studies in the following.

(a) Resonant Electrostatic Fields in Density Gradients

In a density gradient, localized intense electric fields can be generated in regions where plasma resonances exist. These resonances occur where the wave frequency matches the local lower hy-

[11] K. L. McAdams, J. LaBelle, P. W. Schuck, and P. M. Kintner, "PHAZE II Observations of Lower Hybrid Burst Structures Occurring on Density Gradients," *Geophys. Res. Lett.,* **25**, 3091 (1998).

[12] K. A. Lynch, R. L. Arnoldy, P. M. Kintner, P. W. Schuck, J. W. Bonnell, and V. Coffey, "Auroral Ion Acceleration From Lower Hybrid Solitary Structures: A Summary of Sounding Rocket Observations," *J. Geophys. Res.,* **104**, 28515 (1999).

[13] P. M. Kintner, J. Vago, S. Chesney, R. L. Arnoldy, K. A. Lynch, C. J. Pollock, and T. E. Moore, "Localized Lower Hybrid Acceleration of Ionospheric Plasma," *Phys. Rev. Lett.,* **68**, 2448 (1992).

[14] J. L. Vago, P. M. Kintner, S. Chesney, R. L. Arnoldy, K. A. Lynch, T. E. Moore, and C. J. Pollock, "Transverse Ion Acceleration by Localized Lower Hybrid Waves in the Topside Auroral Ionosphere," *J. Geophys. Res.,* **97**, 16935 (1992).

[15] K. A. Lynch, R. L. Arnoldy, P. M. Kintner, and J. Bonnell, "The AMICIST Auroral Sounding Rocket: A Comparison of Transverse Ion Acceleration Mechanisms," *Geophys. Res. Lett.,* **23**, 3293 (1996); and J.-L. Pincon, P. M. Kintner, P. W. Schuck, and C. E. Seyler, "Observation and Analysis of Lower Hybrid Solitary Structures as Rotating Eigenmodes," *J. Geophys. Res.,* **102**, 17283 (1997).

[16] R. E. Ergun, C. W. Carlson, J. P. McFadden, F. S. Mozer, G. T. Delory, W. Peria, C. C. Chaston, M. Temerin, I. Roth, L. Muschietti, R. Elphic, R. Strangeway, R. Pfaff, C. A. Cattell, D. Klumpar, E. Shelley, W. Peterson, E. Moebius, and L. Kistler, "FAST Satellite Observations of Large-Amplitude Solitary Structures," *Geophys. Res. Lett.,* **25**, 2041 (1998); and R. E. Ergun, C. W. Carlson, J. P. McFadden, F. S. Mozer, L. Muschietti, I. Roth, and R. J. Strangeway, "Debye-Scale Plasma Structures Associated With Magnetic-Field-Aligned Electric Fields," *Phys. Rev. Lett.,* **81**, 826 (1998).

brid frequency or the upper hybrid frequency. The resonance structure can be determined from the spatial evolution of the electric field in an inhomogeneous cold plasma. If we assume a cylindrical density depression with its radial density variation being across the geomagnetic field, then the exact differential equation describing the spatial evolution of the electrostatic potential is:[17]

$$\frac{d^2\phi}{dr^2} + \left\{ \frac{1}{r} + \frac{1}{K_\perp}\frac{dK_\perp}{dr} \right\} \frac{d\phi}{dr} + \left\{ \frac{m}{r}\frac{1}{K_\perp}\frac{dK_\times}{dr} - \frac{m^2}{r^2} - k_z^2 \frac{K_\parallel}{K_\perp} \right\} \phi = 0 \tag{7}$$

where we have assumed that the azimuthal, longitudinal, and temporal variations of the fields are of the form $\exp(im\theta + ik_z z - i\omega t)$. Here $K_\perp$, $K_\times$, and $K_\parallel$ are the cold plasma dielectric tensor elements in the absence of collisions:

$$K_\perp = 1 - \frac{\omega_{pe}^2}{\omega^2 - \omega_{ce}^2} - \sum_i \frac{\omega_{pi}^2}{\omega^2 - \omega_{ci}^2} \tag{8}$$

$$K_\times = -\frac{\omega}{\omega_{ce}} \frac{\omega_{pe}^2}{\omega^2 - \omega_{ce}^2} + \sum_i \frac{\omega_{ci}}{\omega} \frac{\omega_{pi}^2}{\omega^2 - \omega_{ci}^2} \tag{9}$$

$$K_\parallel = 1 - \frac{\omega_{pe}^2}{\omega^2} - \sum_i \frac{\omega_{pi}^2}{\omega^2} \tag{10}$$

where ω_{pe} and ω_{pi} are the electron and ion plasma frequencies, respectively, and ω_{ce} and ω_{ci} are the electron and ion cyclotron frequencies, respectively. The plasma and cyclotron frequencies are assumed to have a radial dependence due to the radial variation of the plasma density and the geomagnetic field. Generally the radial scalelength of the density depression is much smaller than the radial scalelength of the geomagnetic field variation, so that the geomagnetic field can be considered constant over the transverse dimension of the density depression. From (7), it is clear that the differential equation for ϕ has a regular singularity at $K_\perp = 0$. This singularity occurs for frequencies ω corresponding to either the lower hybrid resonance frequency ω_{LH} or the upper hybrid resonance frequency ω_{UH}. From (8), for a single ion species plasma, these are approximately given by

$$\omega_{LH}^2 \approx \frac{\omega_{pi}^2 + \omega_{ci}^2}{1 + \left(\omega_{pe}^2/\omega_{ce}^2\right)} \tag{11}$$

$$\omega_{UH}^2 \approx \omega_{pe}^2 + \omega_{ce}^2 \, . \tag{12}$$

In the vicinity of either of these resonances, it is straightforward to show that ϕ has a logarithmic singularity. Thus, in a density gradient, the electric fields will be locally enhanced for frequencies corresponding to the local lower hybrid frequency or the local upper hybrid frequency. To show this for the space plasmas of interest, we have considered a plasma in a uniform magnetic field with a linear electron density profile:

$$n = \begin{cases} n_0, & \text{for } r \le r_1 \\ n_0 + (n_1 - n_0)\left(\dfrac{r - r_1}{r_2 - r_1}\right), & \text{for } r_1 < r < r_2 \\ n_1, & \text{for } r \ge r_2 \end{cases} \tag{13}$$

where n_0 and n_1 are constants. In the regions $r < r_1$ and $r > r_2$, the solution to (7) can be readily expressed in terms of ordinary Bessel functions or modified Bessel functions, depending on whether $K_\parallel/K_\perp$ is less than or greater than zero, respectively. The solutions have to further satisfy that ϕ remains finite as $r \to 0$ and as $r \to \infty$. The complete solution to (7) over the entire density gradient is obtained by requiring that ϕ match onto these Bessel function solutions at $r = r_1$ and $r = r_2$. This then becomes an eigenvalue problem. For fixed frequency ω the eigenvalue is k_z while for fixed k_z the eigenvalue is ω.

[17] W. P. Allis, S. J. Buchsbaum, and A. Bers, *Waves in Anisotropic Plasmas* (M.I.T. Press, Cambridge, Massachusetts, 1963, and the University of Tokyo Press, International Edition, Tokyo, Japan, 1964).

Let us consider a case where ω is such that $K_\perp(r_0) = 0$ for $r_1 < r_0 < r_2$. Then, for $r \leq r_1$ the solution to (7) is of the form:

$$\phi|_{r \leq r_1} \sim \mathrm{J}_m(\psi) \tag{14}$$

where J_m is the Bessel function of the first kind,

$$\psi = k_z \left| \frac{K_\parallel}{K_\perp} \right|^{1/2} r \ . \tag{15}$$

For $r \geq r_2$ the solution to (7) is of the form:

$$\phi|_{r \geq r_2} \sim \mathrm{K}_m(\psi) \tag{16}$$

where K_m is the modified Bessel function of the first kind. The solution to (7) which matches onto the homogeneous plasma solutions (14) and (15) solves for the eigenvalue k_z. For illustrative purposes, let us assume the following parameters which correspond to the plasma conditions in the auroral ionosphere around an altitude of 1000 km:[13] $n_0 = 3.4 \times 10^9$ m^{-3}, $n_1 = 4.3 \times 10^9$ m^{-3}, singly charged oxygen O^+ and hydrogen H^+ ions with the density ratio of 9:1, respectively, and $B_0 = 0.36$ Gauss. For a fixed ω corresponding to $K_\perp(r_0) = 0$ for $r_1 < r_0 < r_2$ we solve, numerically, (7) for the eigenvalue k_z. It is worth noting that k_z will depend on ω and the width of the gradient region $\Delta r = r_2 - r_1$ and not on the specific values of r_2 and r_1. We find, numerically, that for a given ω and Δr there are two distinct k_z's which satisfy the boundary conditions. For $\Delta r = 1$ m and a frequency of $f_{LH} = \omega/2\pi = 4.55$ kHz (corresponding to the lower hybrid resonance being halfway up the density gradient), the two eigenvalues are $k_{z1} = (0.022 + 0.006i)$ m^{-1} and $k_{z2} = (0.011 - 0.008i)$ m^{-1}. Figure 4 shows the magnitude of the radial electric field $|E_r|$ for $k_z = k_{z1}$. If we choose

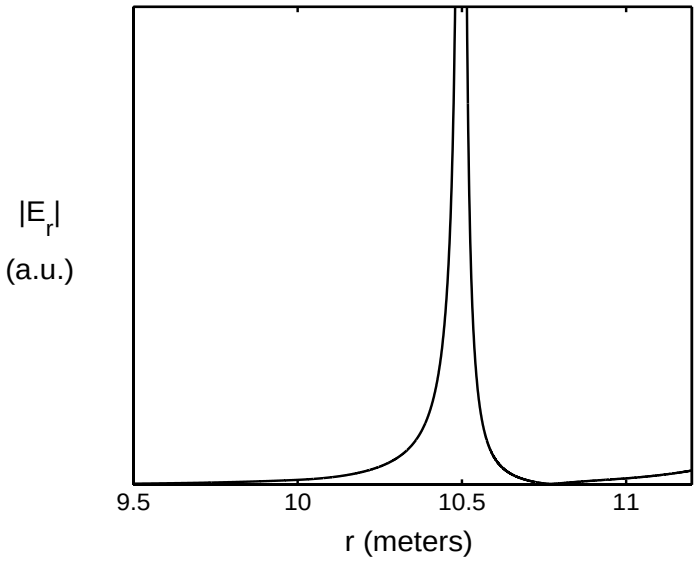

Figure 4: The magnitude of the radial electric field (in arbitrary units) as a function of the distance.

$\Delta r = 10$ m and the same frequency, then the two eigenvalues are $k_{z1} = (0.029 + 0.3i)$ m^{-1} and $k_{z2} = (0.023 - 0.02i)$ m^{-1}. Thus, the lower hybrid fields propagate along the geomagnetic field for sharp density gradients and are essentially evanescent for more gradual density gradients. It is worth noting that even when the imaginary part of k_z is small compared to the real part, the fields are not "propagating" over long distances before damping out spatially. The spatial extents are

typically of the order of 100 m. These distances are relatively short compared to what is inferred from observations.[18] Hence such fields would have to be maintained by a source of free energy (e.g., an independent streaming instability) inside the density depleted region.

(b) Interaction of Ions With Localized Fields

The interaction of ions with localized field structures is different from that with a plane wave or a set of plane waves, which we have studied in the past.[19] The primary difference is that since these structures are smaller than the ion Larmor radius, the interaction of the ions with the fields occurs over only a small fraction of their orbit. We have done some preliminary studies of ion orbits in some idealized localized fields.

Let us consider the situation in which the wave fields are independent of the coordinate along the geomagnetic field. We can then consider just the motion of the ions in a plane perpendicular to the geomagnetic field. For an ion in a uniform magnetic field ($\vec{B} = B_0\hat{z}$) interacting with electrostatic waves propagating along $\hat{x}$, the equations of motion are:

$$\frac{dx}{dt} = v_x \tag{17}$$

$$\frac{dv_x}{dt} = \Omega v_y + \frac{Q}{M}E(x,y,t) \tag{18}$$

$$\frac{dy}{dt} = v_y \tag{19}$$

$$\frac{dv_y}{dt} = -\Omega v_x \tag{20}$$

where Ω is the angular ion cyclotron frequency, and Q and M are the charge and mass of the ion, respectively. Consider the following special case of a spatially localized electric field

$$E(x,y,t) = \left[\sum_i E_i \sin\left(\phi_i - \omega_i t\right)\right] \delta\left(\frac{r}{a} - 1\right) \tag{21}$$

where a is the radius of the cavity, $r^2 = x^2 + y^2$, and ϕ_i is an arbitrary phase of the i-th field component of magnitude E_i and frequency ω_i. The equations of motion can be integrated numerically to determine the effect of the localized fields on the ion orbits. For illustrative purposes, we have chosen the upper ionospheric parameters discussed in part (a). We assume that $a = 10$ m, $B_0 = 0.36$ Gauss, and consider a single component with an amplitude of 20 mV/m and frequency of 5 kHz. Then the ratio of the wave frequency to the O^+ and H^+ cyclotron frequencies is, respectively:

$$\frac{f_{\rm wave}}{f_{cO^+}} = 146.2, \qquad \frac{f_{\rm wave}}{f_{cH^+}} = 9.1\ . \tag{22}$$

For an ambient temperature of 0.33 eV, the initial Larmor radii of the two ion species are, respectively:

$$\rho_{O^+} \approx 6.5\ {\rm m}, \qquad \rho_{H^+} \approx 1.6\ {\rm m}\ . \tag{23}$$

The numerical results presented below are for O^+ and H^+ ions with their initial Larmor radii as given in (23). Figure 5 shows the orbit of an O^+ ion in the x-y plane as it interacts with the localized field (represented by the dotted curve). It is clear that the Larmor radius of the ion is changing due

[18] R. L. Arnoldy, K. A. Lynch, P. M. Kintner, J. Vago, C. J. Pollock, and T. E. Moore, "Transverse Ion Acceleration and Auroral Electron Precipitation," *Adv. Space Res.,* **13**, 143 (1993).

[19] A. K. Ram, D. Bénisti, and A. Bers, "Ion Acceleration in Multiple Electrostatic Waves," *J. Geophys. Res.,* **103**, 9431 (1998); D. Bénisti, A. K. Ram, and A. Bers, "Ion Dynamics in Multiple Electrostatic Waves in a Magnetized Plasma — Part I: Coherent Acceleration," *Phys. Plasmas,* **5**, 3224 (1998); and D. Bénisti, A. K. Ram, and A. Bers, "Ion Dynamics in Multiple Electrostatic Waves in a Magnetized Plasma — Part II: Enhancement of the Acceleration," *Phys. Plasmas,* **5**, 3233 (1998).

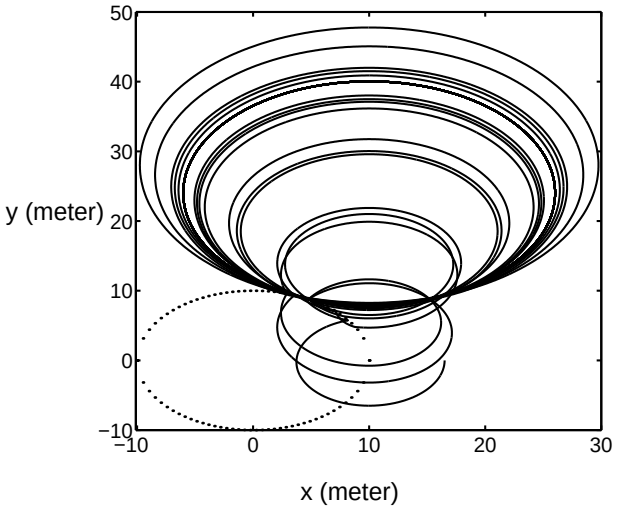

Figure 5: The ion orbit for an O^+ ion. The dots mark the region of the fields.

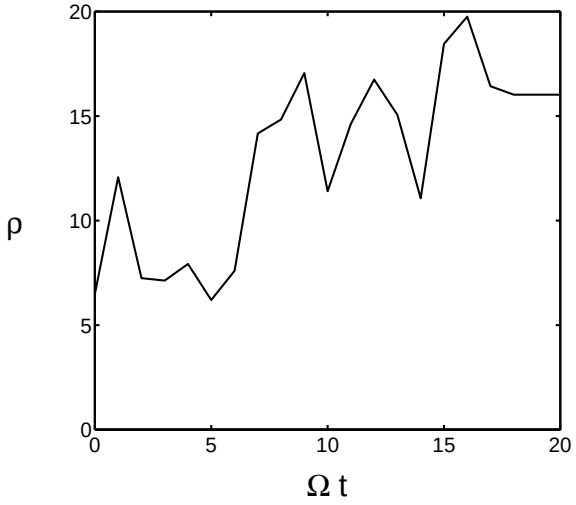

Figure 6: Larmor radius as function of the normalized time.

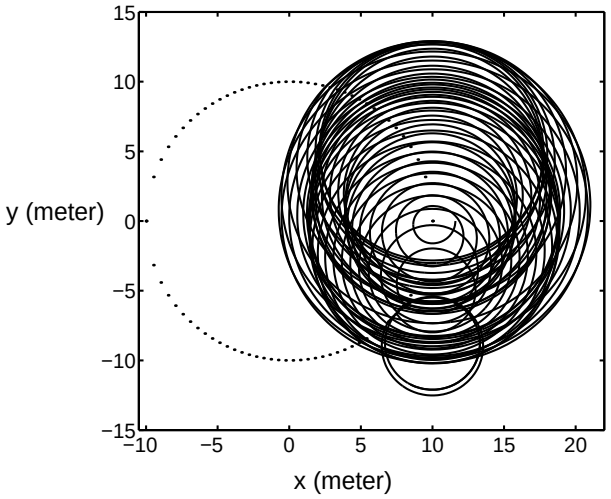

Figure 7: The ion orbit for a H^+ ion. The dots mark the region of the fields.

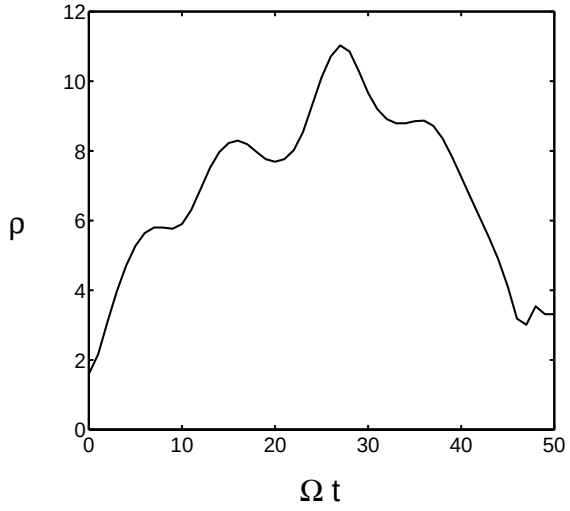

Figure 8: Larmor radius as function of the normalized time.

to this interaction. Figure 6 shows the Larmor radius (in meters) as a function of the normalized time. The ion stops gaining energy after about $\Omega t = 18$. At this point the gyro center of the ion has been shifted, due to its interaction with fields, to such a point that it stops interacting with the fields (the orbit essentially becomes tangential to the field structure). Figures 7 and 8 show the interaction of a H^+ ion with the same field structure. Note that this time the ion gets energized and then de-energized till at the end, when it stops interacting with the fields, the energy is not very different from its initial energy. Figure 9 shows the evolution of the Larmor radius of another H^+ ion (with different initial phase) interacting with the fields. Here the H^+ ion initially gains energy, almost monotonically, before settling at a much higher energy ($\rho \approx 17$ m) than at the start. At a later time $(\Omega t \approx 4000)$, it again monotonically gains energy. The comparison of Figures 9 and 8 shows that the interaction with localized fields leads to a chaotic trajectory of the ions — the energization is very dependent on the initial conditions. The monotonic increases in energy are akin to Lévy flights that have been conjectured and studied for field-particle interactions with a different form for the fields.[20] The Lévy flights of ions will lead to long tails in the ion distribution function, and this could be detected by particle instruments on satellites and rockets.

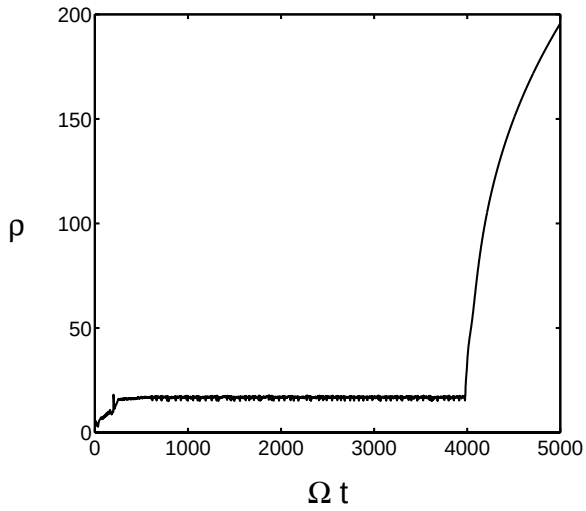

Figure 9: The Larmor radius of a H^+ ion as function of the normalized time.

[20] V. V. Afanasiev, R. Z. Sagdeev, and G. M. Zaslavsky, "Chaotic Jets With Multifractal Space-Time Random Walk," *Chaos,* **1**, 143 (1991); K. Kupfer, A. Bers, and A. K. Ram, "Guiding Center Stochasticity and Transport Induced by Electrostatic Waves," *Research Trends in Physics: Nonlinear and Relativistic Effects in Plasmas,* ed. V. Stefan (New York: American Institute of Physics), 1992, pp. 670–715; and S. D. Schultz, A. Bers, and A. K. Ram, "Anomalous Electron Streaming Due to Waves in Tokamak Plasmas," *Proceedings of the 10th Topical Conference on Radio Frequency Power in Plasmas,* Boston, Massachusetts, April 1–3, 1993, A.I.P. Conf. Proc. 289 (eds. M. Porkolab, J. Hosea), New York (1994), pp. 433–436.

4. Saturation of Stimulated Raman Backscattering with Varying Ion Acoustic Wave Damping

Sponsors

Los Alamos National Laboratory
Grant E29060017-8F

Project Staff

Ante Salcedo, Professor Abraham Bers, Dr. Abhay K. Ram

Stimulated Raman scattering (SRS) of laser power in laser-plasma interactions is an important limiting mechanism for inertial confinement fusion. The linear evolution of SRS is a parametric instability in which the laser's electromagnetic wave (EMW) couples nonlinearly to both an electron plasma wave (EPW) and a scattered, electromagnetic wave (SEMW). The instability growth rate is largest when the SEMW is backward (BEMW), i.e., opposite to the direction of the laser pump EMW; the interaction is then known as the backscattered SRS (BSRS).

The nonlinear saturation of SRS can occur through several mechanisms: nonlinear steepening of the EPW; electron trapping in the EPW; and nonlinear coupling of the EPW to ion-acoustic waves (IAW) through the so-called Langmuir decay parametric instability (LDI). In the last few years, considerable attention has been given to the LDI mechanism, particularly through large-scale numerical simulation techniques restricted to homogeneous plasmas. To better understand this particular saturation mechanism, we have in the past studied analytically and computationally a simplified model of the coupling of SRS to IAW.[21] The simplified model is based upon the following observations: (a) the LDI is driven by the growing EPW in SRS; (b) above threshold, the LDI growth rate exceeds the growth rate of SRS; and (c) the LDI, driven by a growing EPW which decays nonlinearly to a damped EPW (DEPW) and a damped IAW (DIAW), saturates by spatiotemporal chaos (STC), as established in the Ph.D. thesis of C. Chow in our group.[22] In STC, the EPW is randomized so that SRS attains a saturated state given by the laser EMW scattering off a saturated spectrum of EPW's due to LDI. In this calculation, the effects of plasma inhomogeneity could be easily accounted for. Applying this model to particular LPI experiments,[23] we found that the SRS reflectivity scaled with laser intensity as in the experiments.

More recently, experiments have been carried out showing a strong dependence of SRS reflectivity upon the damping of IAW.[24] In different experiments, both increases and reductions in SRS reflectivity with increased IAW damping have been observed and to-date not explained. In the following, we report our first results on using an LDI-STC saturation model to attempt an understanding of these very recent experiments.

---

[21] A. K. Ram, C. Chow, and A. Bers, "Saturation of SRS by Spatiotemporal Chaos in Coupled Langmuir Decay," *Proceedings of the 21st European Physical Society (EPS) Conference on Controlled Fusion and Plasma Physics,* Montpellier, France, June 27– July 1, 1994, Vol. III, pp. 1460–1463.

[22] C. Chow, "Spatiotemporal Chaos in the Nonlinear Three Wave Interaction," Ph.D. thesis, M.I.T. Department of Physics (1991); C. Chow, A. Bers and A. K. Ram, "Spatiotemporal Chaos in the Nonlinear Three Wave Interaction," *Phys. Rev. Lett.,* **68**, 3379 (1992); C. Chow, "Spatiotemporal Chaos in Nonintegrable Three-Wave Interactions," *Physica D,* **81**, 237 (1995).

[23] R. P. Drake et al., "Studies of Raman Scattering From Overdense Targets Irradiated by Several Kilojoules of 0.53 mu m Laser Light," *Phys. Fluids,* **31**, 3130 (1988); R. P. Drake et al., "Hydrodynamic Expansion of Exploding-Foil Targets Irradiated by 0.53 mu m Laser Light," *Phys. Fluids B,* **1**, 1089 (1989).

[24] J. Fernandez et al., "Observed Dependence of Stimulated Raman Scattering on Ion-Acoustic Damping in Hohlraum Plasmas," *Phys. Rev. Lett.,* **77**, 2702 (1996); R. K. Kirkwood et al., "Observation of Multiple Mechanisms for Stimulating Ion Waves in Ignition Scale Plasmas," *Phys. Plasmas,* **4**, 1800 (1997).

Considering LDI as an independent process, where the EPW driven by SRS is a growing wave, the equations for the three-wave interaction, describing LDI, take the following form:

$$\left(\partial_t + \upsilon_3\partial_x - \gamma_{net} - iV\partial_x - D\partial_x^2\right)a_3(x,t) = -Ka_4a_5\,, \tag{24}$$

$$\left(\partial_t + \upsilon_4\partial_x + \gamma_4\right)a_4(x,t) = K^*a_3a_5^*\,, \tag{25}$$

$$\left(\partial_t + \upsilon_5\partial_x + \gamma_5\right)a_5(x,t) = K^*a_3a_4^*\,. \tag{26}$$

In these equations, a_3, a_4 and a_5 are the wavepacket amplitudes of the EPW, DEPW and DIAW, respectively. The wave action density of each mode is given by $\left|a_\ell\right|^2$. The $\upsilon's$ are the group velocities, K is the LDI nonlinear coupling coefficient, γ_4 and γ_5 are the Landau damping rates of the DEPW and DIAW, respectively, and $\gamma = -\gamma_{net} - iV\partial_x - D\partial_x^2$ accounts for the total growth/damping of the EPW driven by SRS.

A careful description of the EPW growth/damping in (24) is necessary to limit the otherwise uncontrolled growth of short wavelengths in our model. This is obtained by expanding the imaginary part of the frequency $\omega_i(k_3)$ from the exact EPW dispersion relation, in the vicinity of k_3, to obtain its non-local representation: $-\gamma_3 a_3 - iV\partial_x a_3 - D\partial_x^2 a_3$, where, $\gamma_3 = \left|\omega_i(k_3)\right|$, $V = \left|\omega'_i(k_3)\right|$, $D = \left|\omega''_i(k_3)\right|/2$, and the primes denote derivatives respect to k_3. The net growth of the EPW is calculated as $\gamma_{net} = (-\gamma_3 + \sqrt{\gamma_3^2 + 4\gamma_{SRS}^2})/2$, where the growth rate of SRS is given by $\gamma_{SRS} = (k_3\upsilon_{o1}/4)\left(\omega_p^2/\omega_2\omega_3\right)^{1/2}$, and $\upsilon_{o1} = eE_1/m_e\omega_1$ is the electron quiver velocity in the laser EMW at $\omega = \omega_1$.

Typically, one has $\upsilon_5 << \upsilon_3$ and $\upsilon_4 \approx -\upsilon_3$. Transforming to the frame moving with the group velocity of the EPW (υ_3), and normalizing length, time, wave amplitudes and damping coefficients as $(\gamma_{net}/\upsilon_3)x \to x$, $\gamma_{net}t \to t$, $(K/\gamma_{net})a_\ell \to a_\ell$, $\gamma_\ell/\gamma_{net} \to \gamma_\ell$, $\upsilon_\ell/\upsilon_3 \to \upsilon_\ell$ and $\left(\gamma_{net}/\upsilon_3^2\right)D \to D$, we obtain the following set of transformed and normalized equations:

$$\left(\partial_t - 1\right)a_3 = -a_4a_5 + D\partial_x^2 a_3 + iV\partial_x a_3\,, \tag{27}$$

$$\left(\partial_t - 2\partial_x + \gamma_4\right)a_4 = a_3a_5\,, \tag{28}$$

$$\left(\partial_t - \partial_x + \gamma_5\right)a_5 = a_3a_4\,. \tag{29}$$

We have numerically integrated (27)–(29) in periodic boundary conditions for the following parameters: $I_o = 5*10^{14}\,Watts/cm^2$, $\lambda = 0.35\,\mu m$, $T_e = 1\,keV$, $n = 0.075n_{cr}$, assuming a fully ionized C_5H_{12} plasma, as in some of the experiments quoted. For these parameters we find $\gamma_4 = 0.3$, $D = 0.015$, and $V = 0.147$. The time evolution of the space-averaged wave action

densities, with $\gamma_5/\gamma_4 = 0.24$ and $\gamma_5/\gamma_4 = 1.96$, are shown in Figure 10. In this figure, we can appreciate that the wave action densities initially grow, at the rate given by γ_{net}, then evolve into a nonlinear state and finally reach a saturated steady state. The saturation of the LDI occurs after twenty to forty normalized time units ($\approx 3\ to\ 6\ ps$).

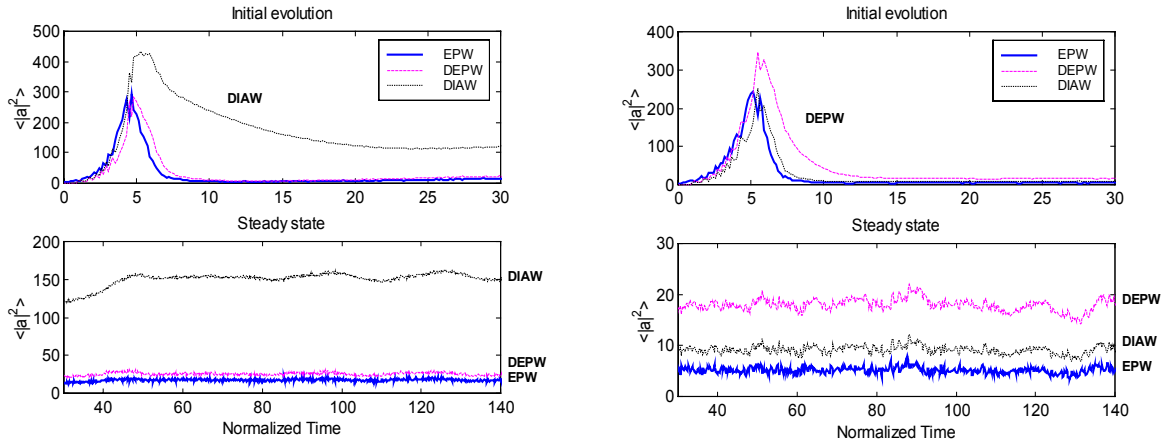

(a) (b)

Figure 10: Time evolution of wave action densities for (a) γ_5/γ_4=0.24 and (b) γ_5/γ_4=1.96.

We have studied the dependence of the saturated steady state on the ion acoustic wave damping, by running different simulations where γ_5/γ_4 was changed. We find that the amplitude of the saturated EPW increases as the damping of the IAW increases, provided that this damping is smaller than the damping of the DEPW. In the opposite case, the amplitude of the EPW decreases as the damping of the ion acoustic wave increases.

The spatial correlation of the steady-state EPW a_3 due to LDI changes in amplitude and width as the IAW damping changes. However, the width remains finite and much smaller than the size of the simulation box, implying the existence of spatial structures that are characteristic of the STC.[22]

Finally, considering the STC-saturated EPW (a_3) in LDI, and assuming an undepleted laser pump, we find the equation for the reflected wave amplitude a_2. For an inhomogeneous plasma with a linear density gradient, this equation reduces to:

$$\upsilon_R \frac{\partial}{\partial x} a_2(x,t) = \Gamma a_1 a_3^*(x,t)\, e^{i\bar{\kappa}' x^2/2}, \qquad (30)$$

where a_1 is the laser EMW amplitude, a_3 is the saturated STC EPW due to LDI, Γ is the SRS coupling constant, $\bar{\kappa}'$ is the linear phase mismatch given by $\kappa' x = k_1 - k_2 - k_3$, $\upsilon_R = (\upsilon_2 - \upsilon_3)/\upsilon_3$, and (30) has been normalized and transformed as (27)–(29).

Direct integration of (30), with a_3 obtained from the steady-state correlation spectrum from the numerical solution of (27)–(29), gives the amplitude of the SRS backscattered electromagnetic wave:

$$a_2(t) = \frac{\Gamma a_1}{\upsilon_R} \int_0^L a_3^*(x,t) e^{i\bar{\kappa}' x^2/2} dx \,. \tag{31}$$

The average SRS reflectivity is then given by:

$$\langle R_{SRS} \rangle \approx \frac{\left\langle |a_2(x,t)|^2 \right\rangle}{|a_1(x,t)|^2} \frac{\omega_1}{\omega_2} \,, \tag{32}$$

where $\langle ... \rangle$ denotes the time average.

We have numerically evaluated (31) for different values of γ_5/γ_4, with the assumption that $\ell_o << 1/\sqrt{\bar{\kappa}'} << L$, where ℓ_o is the correlation width, and L is the box-size of our simulation. Figure 11 shows the obtained SRS reflectivity, normalized to $\langle R_o \rangle$, the reflectivity at $\gamma_5/\gamma_4 = 0.08$ (which approximately corresponds to T_i=0 and hence no ion-Landau damping in the IAW). For $\gamma_5/\gamma_4 \le 1$, the relative SRS reflectivity increases as the ion-acoustic wave damping increases. For $\gamma_5/\gamma_4 \ge 1$, however, the relative SRS reflectivity decreases as the ion acoustic wave damping is increased.

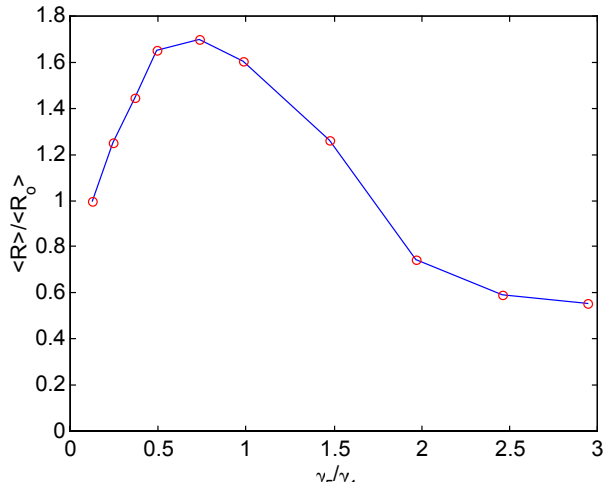

Figure 11: Relative SRS reflectivity as a function of γ_5/γ_4.

5. Electromagnetic Decay Instability in Single Hot Spot Geometry

Sponsors

Los Alamos National Laboratory
Grant E29060017-8F

Project Staff

Ronald J. Focia, Professor Abraham Bers, Dr. Abhay K. Ram

We report on our study of the electromagnetic decay instability (EDI) in a finite geometry. EDI is the decay of a Langmuir (or electron plasma) wave, generated for example by stimulated Raman scattering (SRS), into an electromagnetic wave and an ion acoustic wave. The analysis focused on the finite geometry and inhomogeneous beam intensity of a single hot spot used in recent laser plasma interaction experiments.[25] These experiments are in direct support of the inertial confinement fusion program.

High intensity smoothed laser beams have an intensity profile composed of many speckles or "hot spots." Studying laser plasma interactions (LPI) in a single hot spot (SHS) is fundamental to understanding LPI in smoothed high-intensity beams where LPI takes place in many hot spots. A unique experimental campaign is currently underway at Los Alamos National Laboratory (LANL) in which LPI in a single hot spot is simulated by producing a near diffraction-limited laser beam (see Figure 12) which interacts with a preformed plasma. The geometry of the preformed plasma and near diffraction-limited interaction beam is shown in Figure 13.

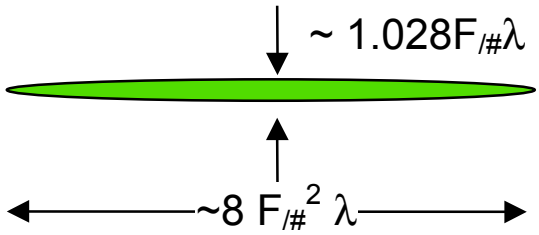

Figure 12. Diffraction-limited laser beam hot spot dimensions. The optic F-number $F_{/\#}$ = f/d, where f is the focal length and d is the aperature, and λ is the wavelength of the laser light. In these experiments λ = 527 nm.

EDI is a resonant three-wave interaction in which the electron plasma wave (EPW) generated from SRS acts as the pump wave for generation of an electromagnetic wave (EMW) and an ion acoustic wave (IAW). In a similar three wave interaction called the Langmuir decay instability (LDI) the EPW pump acts to generate another EPW and an IAW. The growth rate of the EPW pump from SRS is maximized in backward SRS scattering; associated with this is an EPW in the direction of the laser. The amplitude of the EPW pump is assumed to grow exponentially until a

[25] D. S. Montgomery et al., "Characterization of Plasma and Laser Conditions for Single Hot Spot Interaction Experiments," *Laser Part. Beams,* **17**, 349 (1999).

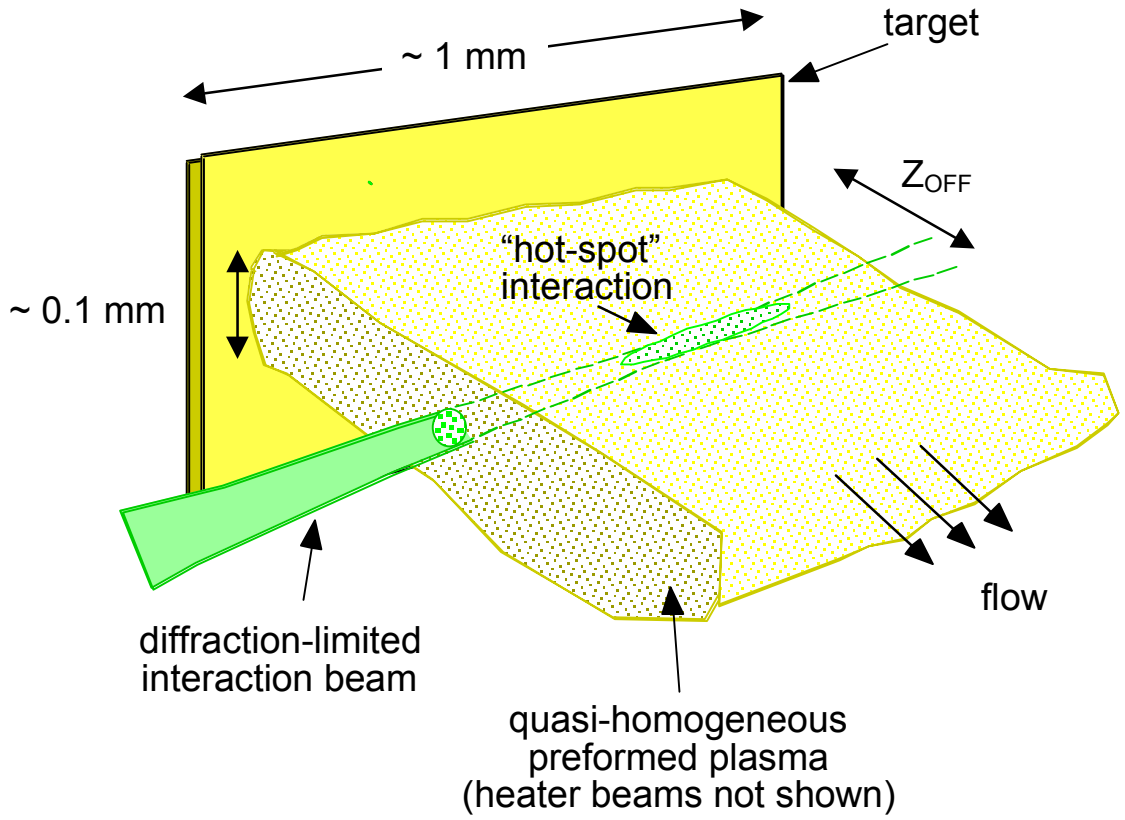

Figure 13. Geometry of the preformed plasma and near diffraction-limited interaction beam.

time t_D when pump depletion of the laser becomes important. The maximum expected EPW pump electric field amplitude that is assumed in the analysis is given by

$$\left|E_{EP}(t_D)\right| \approx 2\left(\frac{n_e}{n_{crit}}\right)^{\frac{1}{4}}\left|E_L\right|, \tag{33}$$

where n_e is the electron density, n_{crit} is the critical density above which electromagnetic waves will not propagate, and E_L is the laser electric field amplitude.

The dispersion relation for EDI is given by

$$\left(\omega_{IA}^2 - c_s^2 k_{IA}^2\right)\left(\omega_{EM}^2 - \omega_{pe}^2 - c^2 k_{EM}^2\right) = \frac{1}{4}\frac{V_{EP}^2}{V_{Te}^2}\omega_{pe}^2\omega_{IA}^2\left(\hat{e}_{EP}^* \bullet \hat{e}_{EM}\right)^2. \tag{34}$$

Since the EMW electric field is perpendicular to its direction of propagation (*k*-vector), the growth of EDI is maximized when the scattered EMW *k*-vector is perpendicular to the EPW pump *k*-vector, and zero when they are colinear. For intermediate angles θ the growth rate will vary like $\sin^2\theta$. In relation to the single hot spot geometry, growth of EDI is maximized in the direction of the shortest interaction length. Although this length is clearly too short for significant convective growth, it is of interest to determine the conditions for an unstable normal mode in which EDI would be an absolute, rather than a convective, instability.

Ignoring dephasings due to plasma inhomogeneity, the linear evolution of EDI in three dimensions can be described by the coupled mode equations

$$\left(\frac{\partial}{\partial t}+\vec{v}_1\bullet\vec{\nabla}+\nu_1\right)a_1=\gamma(\vec{r})a_2^*, \text{ and} \tag{35a}$$

$$\left(\frac{\partial}{\partial t}+\vec{v}_2\bullet\vec{\nabla}+\nu_2\right)a_2=\gamma(\vec{r})a_1^*, \tag{35b}$$

where a constant pump amplitude has been assumed, a_i are the mode action densities, v_i are the group velocities, ν_i are the mode dampings, and γ is the growth rate. Additionally, the plasma is assumed to be homogeneous and the laser intensity constant over the finite extent of the region of interaction. Thus, for the maximum pump amplitude γ is taken constant over the region of interaction and zero outside of this region.

The problem can be reduced to 1D by realizing that the Green's function for the interaction is non-zero only along a line joining the group velocities and then transforming to a coordinate system that has one axis moving with a velocity along this line.[26] The procedure is outlined in the following and illustrated in Figure 14 for the two-dimensional case. First one rotates the coordinate system by the angle θ so that one axis is orthogonal to the boundary; then one

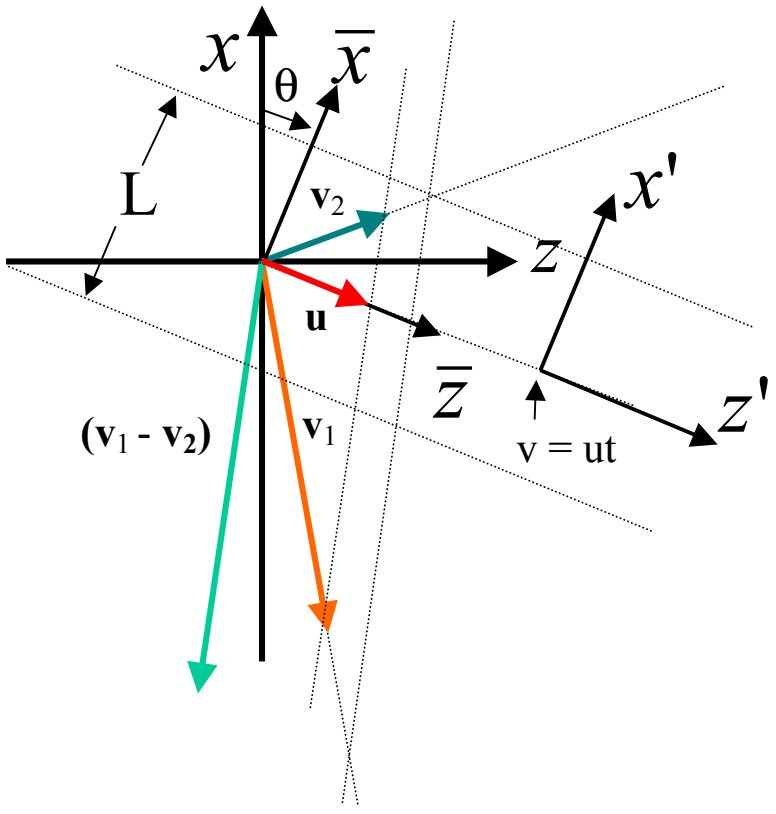

Figure 14. Geometry of the coordinate transformations.

[26] A. Reiman, "Parametric Decay in a Finite Width Pump, Including the Effects of Three-Dimensional Geometry and Inhomogeneity," *Phys. Fluids,* **21**, 1000 (1978).

transforms to a non-orthogonal coordinate system moving along the pump. Applying these transformations to (35), one obtains

$$\left(\frac{\partial}{\partial t'} + \mathrm{v}_{1x'}\frac{\partial}{\partial x'} + \nu_1\right)a_1 = \gamma a_2^* \tag{36a}$$

$$\left(\frac{\partial}{\partial t'} + \mathrm{v}_{2x'}\frac{\partial}{\partial x'} + \nu_2\right)a_2 = \gamma a_1^* \tag{36b}$$

Assuming a time dependence $a_{1,2} \sim e^{pt}$, the solution to the system of equations (36) in the finite extent L is well-known[27] and given by the trancendental equation

$$P\tan\left[\left(1-P^2\right)^{\frac{1}{2}}\alpha L\right] + \left(1-P^2\right)^{\frac{1}{2}} = 0\,, \tag{37}$$

where

$$\mathrm{P} = \frac{\mathrm{p}}{\mathrm{p_o}} + \frac{\gamma_a}{\gamma}\,, \tag{38}$$

$$\mathrm{p_o} = \frac{2\left|\mathrm{v}_{1\bar{x}}\mathrm{v}_{2\bar{x}}\right|^{\frac{1}{2}}}{\left|\mathrm{v}_{1\bar{x}}\right| + \left|\mathrm{v}_{2\bar{x}}\right|}\gamma\,, \tag{39}$$

$$\gamma_\mathrm{a} = \frac{\nu_1\left|\mathrm{v}_{2\bar{x}}\right| + \nu_2\left|\mathrm{v}_{1\bar{x}}\right|}{2\left|\mathrm{v}_{1\bar{x}}\mathrm{v}_{2\bar{x}}\right|^{\frac{1}{2}}}\,, \tag{40}$$

$$\alpha = \frac{\gamma}{\left|\mathrm{v}_{1\bar{x}}\mathrm{v}_{2\bar{x}}\right|^{\frac{1}{2}}}\,, \tag{41}$$

and L is the finite length extent perpendicular to the EPW pump.

If the length of interaction L is long enough, an absolute normal mode may exist. If there is no absolute normal mode, then there is merely convective amplification. Since the largest growth for EDI is in the direction of shortest interaction length, there may be little side scatter observed from EDI. For the experimental parameters: $I_L = 10^{15}$ W/cm^2, λ_L = 527 nm, T_e = 500 eV, T_i = 150 eV, n_e/n_{crit} = 0.05, CH plasma, and $F_{/\#}$ = 4.4 we find that the SHS will have a width of 2.38 μm and length of 81.62 μm. Solving (37) for these parameters, we find that the minimum interaction length for a normal mode to exist is 26.7 μm. Thus, for direct side-scattered EDI a normal mode will not exist. If we vary the optic F-number $F_{/\#}$, or laser intensity I_L, holding the other constant, we can find the minimum values necessary for a normal mode exist. Doing so, we find that a normal mode would require $F_{/\#}$ = 49 for $I_L = 10^{15}$ W/cm^2, and $I_L = 1.25\text{x}10^{17}$ W/cm^2 for $F_{/\#}$ = 4.4. The $F_{/\#}$ of 49 is unreasonable as the typical focusing optics and beam diameter result in a range of $F_{/\#}$ = 4-7. However, the intensity of $1.25\text{x}10^{17}$ W/cm^2 is not unreasonable to achieve with currently available lasers and chirped pulse compression techniques. Thus, an unstable normal mode can exist for certain experimental parameters.

[27] A. Bers, pp. 504–506, "Space-Time Evolution of Plasma Instabilities — Absolute and Convective," in *Handbook of Plasma Physics* (gen. eds. M. N. Rosenbluth and R. Z. Sagdeev), *Vol. 1, Basic Plasma Physics* (vol. eds. A. A. Galeev and R. N. Sudan), Chapter 3.2, North-Holland Publishing Co., 1983, pp. 451–517.

6. Publications

Conference Papers

Bers, A. and A. K. Ram. "Energization of Ions by Resonant Electric Fields in Density Gradients." *Bull. Am. Phys. Soc.* 44: 152 (1999).

Focia, R. J., A. Bers, and A. K. Ram. "Electromagnetic Decay Instability in Single Hot Spot Geometry." *Bull. Am. Phys. Soc.* 44: 181 (1999).

Forest, C. B., P. K. Chattopadhyay, M. D. Nornberg, S. C. Prager, M. A. Thomas, E. Uchimoto, A. P. Smirnov, R. W. Harvey, and A. K. Ram. "Radio Frequency Wave Experiments on the MST Reversed Field Pinch." *Proceedings of the 13th Topical Conference on Radio Frequency Power in Plasmas,* Annapolis, Maryland, April 12–14, 1999. Eds. S. Bernabei and F. Paoletti. Woodbury, New York: A.I.P. Conference Proceedings 485, 1999, pp. 193–201.

Ram, A. K., A. Bers, and S. D. Schultz. "Coupling to, and Propagation of, Electron Bernstein Waves in Spherical Tokamaks." *Bull. Am. Phys. Soc.* 44: 186 (1999).

Ram, A. K. "Electron Bernstein Wave Excitation in NSTX-Type High-β Plasmas." *Proceedings of the 13th Topical Conference on Radio Frequency Power in Plasmas,* Annapolis, Maryland, April 12–14, 1999. Eds. S. Bernabei and F. Paoletti. Woodbury, New York: A.I.P. Conference Proceedings 485, 1999, pp. 375–382.

Ram, A. K. and A. Bers. "Generation of, and Ion Energization by, Localized Electric Fields in Density Gradients." *Eos (1999 American Geophysical Union Fall Meeting supplement)* 80: F867 (1999), Paper SM31A-09.

Ram, A. K., and A. Bers. "Ion Energization by Resonant Electric Fields in Density Gradients." *Proceedings of the 5th Interrelation Between Plasma Experiments in Laboratory and Space (IPELS) Conference,* Kreuth, Germany, August 9–13, 1999, p 2.7.

Ram, A. K. and A. Bers. "Ion Energization by Resonant Electric Fields in Density Gradients." *Eos (1999 American Geophysical Union Spring Meeting supplement)* 80: S307 (1999), Paper SM52A-23.

Ram, A. K., A. Bers, and C. N. Lashmore-Davies. "Electron Cyclotron Heating and Current Drive in Spherical Tokamaks." To appear in *Proceedings of the 6th International Spherical Tori (ST) Workshop, The US-Japan Spherical Tori (ST) Workshop, and The US-Japan Workshop on Physics of Innovative High-Beta Fusion Plasma Confinement,* Seattle, Washington, November 19–21, 1999.

Salcedo, A., A. Bers, and A. K. Ram. "Electron-Plasma and Ion-Acoustic Landau Damping in SRS-LDI Saturation." *Bull. Am. Phys. Soc.* 44: 180 (1999).

Salcedo, A., A. Bers, and A. K. Ram. "Saturation of Stimulated Raman Backscattering With Varying Ion Acoustic Wave Damping." *Proceedings of the 1st International Conference on Inertial Fusion Sciences and Applications (IFSA)*, Bordeaux, France, September 12–17, 1999. Elsevier Press, March 2000, Paper W01a3-220.

Schultz, S. D., A. Bers, and A. K. Ram. "Combined RF Current Drive and Bootstrap Current in Tokamaks." *Proceedings of the 13th Topical Conference on Radio Frequency Power in Plasmas,* Annapolis, Maryland, April 12–14, 1999. Eds. S. Bernabei and F. Paoletti. Woodbury, New York: A.I.P. Conference Proceedings 485, 1999, pp. 317–320.

Technical Reports

Ram, A. K. "Acceleration of Ionospheric Ions by Wave-Particle Interactions." PSFC/JA-99-7. Cambridge: M.I.T. Plasma Science and Fusion Center, March 1999.

Ram, A. K. "Electron Bernstein Wave Excitation in NSTX-Type High-β Plasmas." PSFC/JA-99-19. Cambridge: M.I.T. Plasma Science and Fusion Center, June 1999.

Schultz, S. D., A. Bers, and A. K. Ram. "Combined RF Current Drive and Bootstrap Current in Tokamaks." PSFC/JA-99-20. Cambridge: M.I.T. Plasma Science and Fusion Center, June 1999.

Schultz, S. D., A. K. Ram, and A. Bers. "Mode-Converted Electron Bernstein Waves for Heating and Current Drive in NSTX." PSFC/JA-99-6. Cambridge: M.I.T. Plasma Science and Fusion Center, March 1999.

Theses

Schultz, S. D. "Lower Hybrid and Electron Cyclotron Current Drive With Bootstrap Current in Tokamaks." Ph.D. dissertation. Department of Physics, MIT, 1999.